INSTITUTE OF PHYSICS PUBLISHING JOURNAL OF PHYSICS D: APPLIED PHYSICS

J. Phys. D: Appl. Phys. **39** (2006) 1993–2000 doi:10.1088/0022-3727/39/10/002

Effect of thermal annealing on $Fe_{40}Ni_{38}B_{18}Mo_4$ thin films: modified Herzer model for magnetic evolution

T Hysen[1], S Deepa[1], S Saravanan[1], R V Ramanujan[2], D K Avasthi[3], P A Joy[4], S D Kulkarni[4] and M R Anantharaman[1]

[1] Department of Physics, Cochin University of Science and Technology, Cochin 682 022, Kerala, India
[2] School of Materials Engineering, Nanyang Technological University, Singapore 639 798, Singapore
[3] Nuclear Science Centre, Aruna Asaf Ali Marg, New Delhi 110 067, India
[4] Physical Chemistry Division, National Chemical Laboratory, Pune 411 008, India

E-mail: mra@cusat.ac.in

Received 25 December 2005, in final form 27 December 2005
Published 5 May 2006
Online at stacks.iop.org/JPhysD/39/1993

Abstract

Magnetic properties of nano-crystalline soft magnetic alloys have usually been correlated to structural evolution with heat treatment. However, literature reports pertaining to the study of nano-crystalline thin films are less abundant. Thin films of $Fe_{40}Ni_{38}B_{18}Mo_4$ were deposited on glass substrates under a high vacuum of $\approx 10^{-6}$ Torr by employing resistive heating. They were annealed at various temperatures ranging from 373 to 773 K based on differential scanning calorimetric studies carried out on the ribbons. The magnetic characteristics were investigated using vibrating sample magnetometry. Morphological characterizations were carried out using atomic force microscopy (AFM), and magnetic force microscopy (MFM) imaging is used to study the domain characteristics. The variation of magnetic properties with thermal annealing is also investigated. From AFM and MFM images it can be inferred that the crystallization temperature of the as-prepared films are lower than their bulk counterparts. Also there is a progressive evolution of coercivity up to 573 K, which is an indication of the lowering of nano-crystallization temperature in thin films. The variation of coercivity with the structural evolution of the thin films with annealing is discussed and a plausible explanation is provided using the modified random anisotropy model.

(Some figures in this article are in colour only in the electronic version)

1. Introduction

Nano-crystalline alloys obtained by the devitrification of Fe rich metallic glasses have been the subject of intense research ever since their discovery. Since then much attention has been focused on the structural and magnetic features of the bulk amorphous alloys and their changes resulting from various thermal treatments [1]. These alloys are often synthesized by melt quenching techniques with cooling rates often exceeding 10^6 K S^{-1} which are subsequently subjected to heat treatment to induce nanocrystallization [2]. $Fe_{40}Ni_{38}B_{18}Mo_4$ is one such soft magnetic alloy that exhibits superior magnetic properties [3]. Its softness after nanocrystallization can be ascribed to its two phase nature consisting of an ultra-fine grained Fe–Ni phase embedded in the remaining boron rich amorphous matrix [4]. The two phases have Curie temperatures of $\approx$ 760 K and $\approx$ 485 K, respectively, and their contributions to the total saturation magnetizations are $\approx$ 46 emu g^{-1} and $\approx$ 49 emu g^{-1}, respectively. It has room temperature saturation magnetization of 8.8 kG. Its

increased Curie temperature of 626 K and low saturation magnetostriction of 12×10^{-6} accounts for the good soft magnetic properties exhibited by this material. The material can be tailored by field annealing for superior soft magnetic properties such as $H_c = 7$ mOe, $M_r = 7.5$ kG and a dc permeability of about 45000 [5]. These superlative properties has been exploited for various technological applications, namely, sensors, actuators, shielding, high frequency transformer cores, magneto-optic sensors and magnetic recording.

Of particular importance to technological applications is the occurrence of nano-crystallization in the material. Nanocrystallization can be induced in two ways: (i) by annealing just below the crystallization temperature [6] and (ii) by ion/fast-electron irradiation [7]. The latter method is not cost-effective and often difficult to perform. Annealing the sample just above the crystallization temperature can induce crystallization in the sample. In bulk amorphous alloys crystallization at nano-level has been achieved [8], but this has been elusive in the case of thin film magnetic structures.

Amorphous alloys which are precursors for nano-crystalline alloys can be synthesized by several methods, namely, melt quenching, splat cooling, laser glazing, electro-deposition, ion implantation, swift heavy ion irradiation and vapour deposition [9]. Even though plenty of reports exist in the literature on nano-crystalline alloys, there are very few investigations related to the comparative study of properties of bulk amorphous alloys prepared by conventional routes and alloys prepared by novel techniques such as vapour quenching.

In the case of amorphous alloys, the soft magnetic properties exhibited by these materials are explained based on a simple model first proposed by Alben *et al* [10] and later modified by Herzer [11]. The Herzer model, which is generally applicable to bulk materials, suggests that superior soft magnetic properties can be observed in amorphous materials when the exchange correlation length (L_{ex}) is of the order of grain size (D). In such a case the magnetic properties of the samples are greatly enhanced due to the averaging of magneto-crystalline anisotropies 'K_1' over several domains and the sample as such offers very little resistance to coherent domain rotation by an external applied field. Since nano-crystalline materials are widely used for sensor application [12], increasing the surface area would facilitate fabrication of thin film sensors that can be integrated with today's microelectronics. Also, decreasing one or more of the sample dimensions to the order of domain wall width ($\delta \sim$ 40 nm for iron-based alloys) in the bulk material can augment nano-crystallization in the sample at lower temperatures and thereby enhance the magnetic properties. The above conditions can alternatively be realized by depositing ultra-thin layers of metallic glasses on suitable substrates. In this investigation the authors discuss the deposition of thin films of amorphous alloy metglas 2826MB™ on glass substrates and the modification of their magnetic properties with thermal annealing. A modified model based on the Herzer model is proposed to explain the observed soft magnetic property of ultra-thin magnetic films.

2. Experimental methods

2.1. Preparation of metglas thin films

Metglas ribbons having the composition $Fe_{40}Ni_{38}B_{18}Mo_4$ were vacuum-evaporated under high vacuum of (10^{-6} Torr) using tungsten filaments on ultrasonically cleaned glass substrates. Evaporation was carried out quickly so as to keep the film composition as close as possible to that of the bulk ribbon. The thicknesses of the deposited films were also determined using the Dektac 6M Stylus Profiler.

2.2. Annealing

The bulk ribbons were subjected to differential scanning calorimetry (DSC) with a view to determining the crystallization temperatures and their thermal stability. The enthalpy change associated with the phase transformation is calculated by integrating the peak area. The activation energies of crystallization were determined using the Kissinger equation [13]:

$$\ln\left(\frac{b}{T_p^2}\right) = \frac{-E}{k_B T_p} + \ln K. \tag{1}$$

The activation energy E is determined by plotting for a number of scans at different rates b, $\ln(b/T_p^2)$ versus $(1/T_p)$. T_p is the peak temperature, k_B the Boltzman's constant and K a characteristic constant associated with the transformation kinetics . The slope of the linear fit through the data points gives $(-E/k_B)$ from which the activation energy 'E' corresponding to phase formation in the ribbons can be determined. Based on the DSC results the thin film samples were also annealed at different temperatures ranging from 373 to 773 K under high vacuum conditions.

2.3. X-ray diffraction studies

The x-ray diffraction (XRD) spectra of the metglas samples, pristine as well as annealed, were recorded using an x-ray diffractometer (Rigaku D-max-C) using Cu Kα radiation ($\lambda = 1.5418$ Å). The average particle size is determined from the measured width of their diffraction curves using the Debye–Scherrer formula $D = (0.9\lambda/\beta \cos\theta)$, where λ is the wavelength of Cu Kα radiation, β the FWHM, D the average grain size and θ the diffracting angle.

2.4. Atomic force microscopy (AFM) and magnetic force microscopy (MFM) studies

The surface topography of the prepared thin films was studied using a standard AFM (Digital Instruments Nanoscope II) with provisions for MFM imaging. AFM imaging is used to study the microstructure and MFM imaging is used to study the magnetic domain characteristics.

2.5. Vibrating sample magnetometry (VSM) studies

The hysteresis loop parameters, namely saturation magnetization (M_s), coercivity (H_c) and retentivity (M_r) of the metglas samples, were evaluated using a vibrating sample magnetometer (VSM) (model: EG & G PAR 4500) in the parallel and

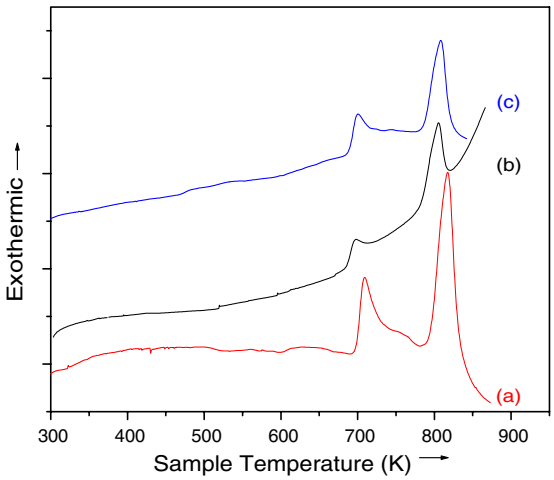

Figure 1. DSC thermogram of metglas ribbons for heating rates (*a*) 20 K min^{-1} (*b*) 10 K min^{-1} and (*c*) 5 K min^{-1}

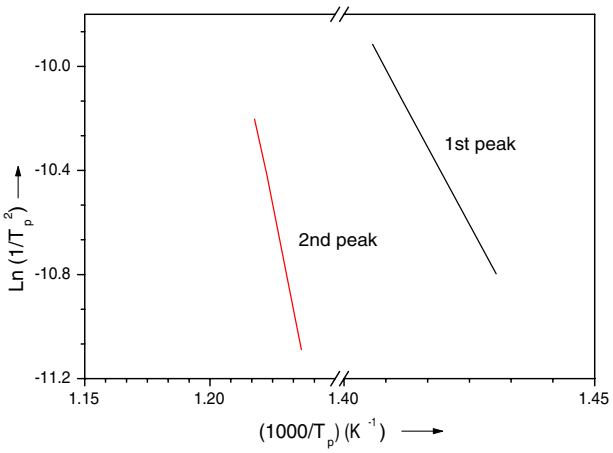

Figure 2. Kissinger plots of the $Fe_{40}Ni_{38}Mo_4B_{18}$ alloy for the two crystalline phase transformations.

perpendicular fields (magnetic field parallel and perpendicular to the film plane) at room temperature for both pristine and annealed thin films.

3. Results and discussion

3.1. Crystallization studies

The DSC studies carried out on these ribbons clearly indicate a two-step devitrification process (figure 1). Two main exothermic peaks were found in the DSC, which corresponds to two stages of crystallization. The first peak rises sharply which indicates spontaneous nucleation and grain growth and the slow growth of second phase suggests sluggish nucleation and growth at the expense of the first phase. The first exotherm which is asymmetric with its trailing end extended on to the high temperature side can be attributed to the devitrification process giving rise to a homogeneously dispersed Fe–Ni nano-phase embedded in a residual boron rich amorphous matrix. This contributes substantially to the magnetic properties of the sample. The second DSC exotherm corresponds to the crystallization of the residual amorphous phase and the precipitation of $FeNiMo_{23}B_6$ [14]. For bulk ribbons, the crystallization temperatures associated with the phases are 699 K for the first phase and 809 K for the second phase for a heating rate of 15 K min^{-1}. These results are in close agreement with that obtained by Du and Ramanujan [15] but differ from that of Nicolai *et al* [16]. Nicolai *et al* found a five-step crystallization in the sample, which may be due to stoichiometric variations. The enthalpy changes associated with crystallization which corresponds to the maximum energy associated with the phase transformations are 13.9 J g^{-1} and 51 J g^{-1}, respectively. The lower enthalpy of formation of the first phase is suggestive of easy nucleation at lower annealing temperatures. The higher enthalpy of the second phase demands higher annealing temperatures and thereby higher thermal energies for nucleation and growth. The Kissinger plots for the two crystalline phases are shown in figure 2. The activation energies for the two phases are 3.07 eV atom^{-1} and 4.09 eV atom^{-1}, respectively. The higher activation energies

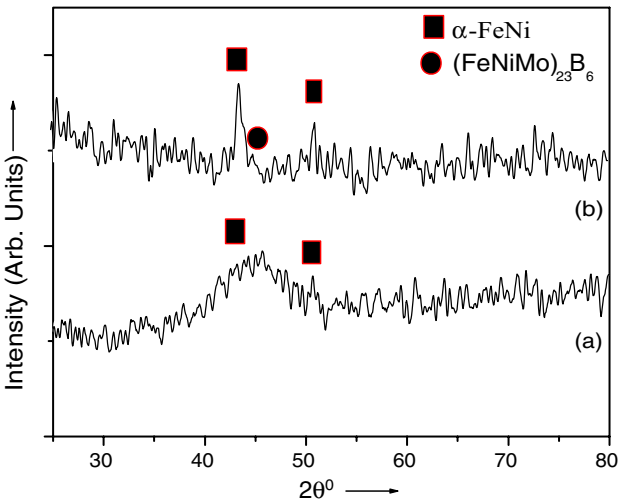

Figure 3. XRD spectrum of metglas ribbons (*a*) un-annealed (*b*) annealed at 773 K.

can be attributed to the presence of less diffusive heavy elements such as molybdenum in the alloy.

3.2. Structural analysis

The thicknesses of the deposited films were also determined using the Dektac 6M Stylus Profiler and were found to be 36 nm.

From figure 3(*a*) it is evident that the as-prepared ribbons are amorphous. The diffraction patterns of the annealed ribbons (figure 3(*b*)) and films (figure 4(*b*)) clearly indicate crystallization in the samples with thermal treatments. Subjecting the ribbons to thermal annealing at 773 K resulted in the precipitation of FeNiMo along with the $FeNiMo_{23}B_6$ phase. Annealing the films at 673 K resulted in the precipitation of nano-crystalline FeNi and cubic boride phases suggesting that the FeNi crystallization occurs at a much lower annealing temperature. The films become more crystalline with thermal treatments at 773 K.

The x-ray diffraction patterns of the as-deposited single layer films with thickness of 36 nm and annealed at 673 K are shown in figures 4(*a*) and (*b*). The pristine films show broad

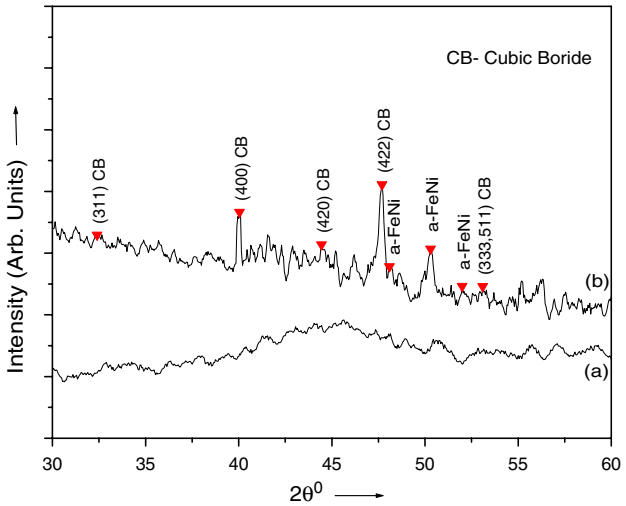

Figure 4. XRD spectrum of metglas thin film (*a*) as-prepared (*b*) annealed at 673 K

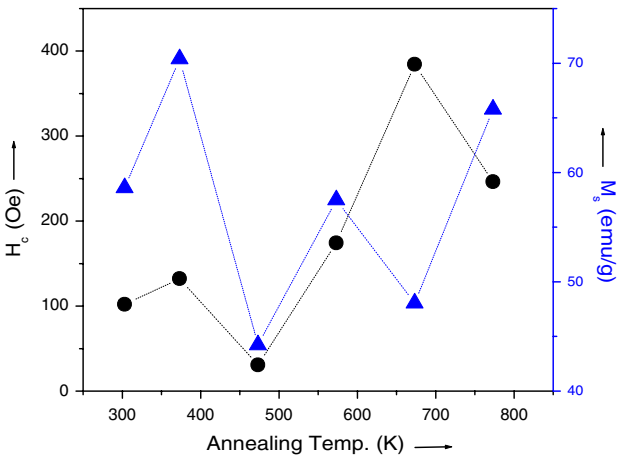

Figure 5. Variation of coercivity and saturation magnetization of metglas thin films for various annealing temperatures. The error bar estimated from the instrument performance at $\pm 0.5\,\mathrm{Am}^{-1}$ is similar to the size of the symbols and is omitted for clarity. (The Lines are guide to the eye.)

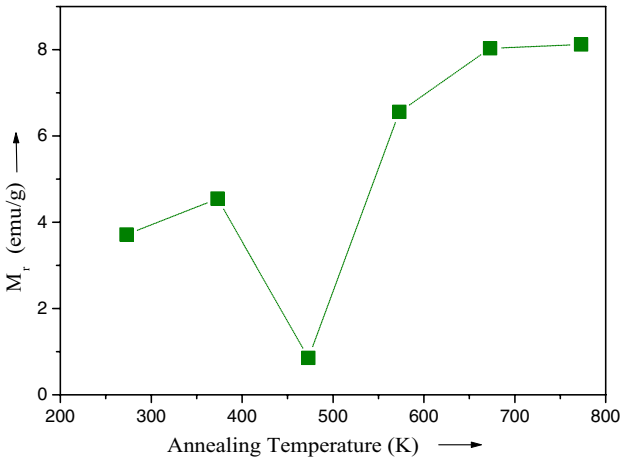

Figure 6. Variation of retentivity with annealing temperature for metglas thin films. (The dotted lines are guide to the eye.)

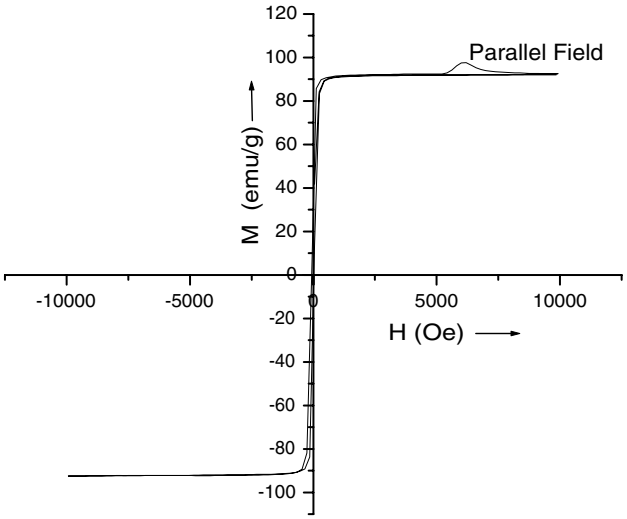

Figure 7. Hysteresis loop behaviour of pristine metglas ribbon in parallel field.

diffraction peaks, which indicate their amorphous nature. But interestingly this is in contradiction to the results reported by Jyothi and Suryanarayana [17], where they found that the as-deposited films are crystalline. The amorphous nature of our samples may be due to their ultra-fine nature. It must also be borne in mind that we have employed the vapour deposition technique rather than flash evaporation. Moreover, since the films are ultra-thin the number of planes contributing to the total x-ray intensity is very small compared with highly crystalline bulk samples/thick films.

3.3. Magnetic characterization

The soft magnetic properties are strongly dependent on the microstructure of the thin films. The microstructure contribution to magnetism arises from morphology, properties such as magnetic anisotropy, magnetostriction, coercivity and the volume fraction of the precipitates. Figures 5 and 6 depicts the variation of soft magnetic properties with thermal treatments. The variation can be attributed to the structural changes occurring in the sample with heat treatments. The sharp drop in coercivity at 473 K represents the onset of crystallization and exchange coupling between several grains. The grain sizes of the dispersed crystallites are rather small resulting in the averaging of magneto-crystalline anisotropies over several domains. The retentivity also reduces, suggesting that ferromagnetic to paramagnetic transition occurs in the interfacial boundary between FeNi and the amorphous matrix in the vicinity of Curie temperature.

Typical hysteresis loops for metglas ribbons and thin films in parallel field (applied external magnetic field parallel to the film plane) are shown in figures 7 and figure 8. The bulk material has a characteristic saturation magnetization of $90.5\,\mathrm{emu\,g}^{-1}$ which corresponds to a saturation magnetic field of 8.8 kG. But the prepared films have lower M_s values suggesting that the homogeneous precipitation of α-FeNiMo cannot be realized by vapour deposition. Evidently vapour deposition alters the stoichiometry and results in phase segregation. By lowering the nano-crystallization temperature in the deposited thin films and considering the

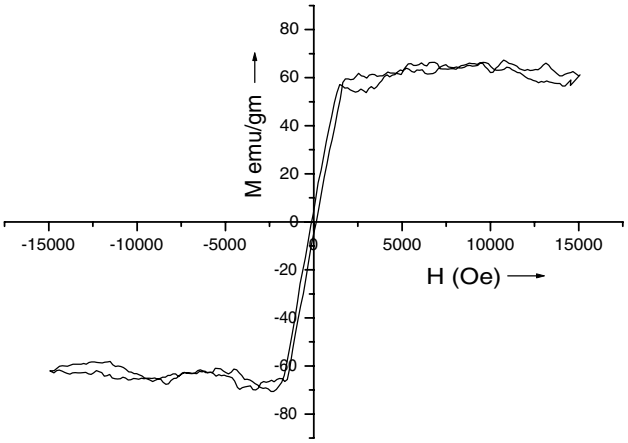

Figure 8. Typical hysteresis loop for pristine metglas thin film in parallel field.

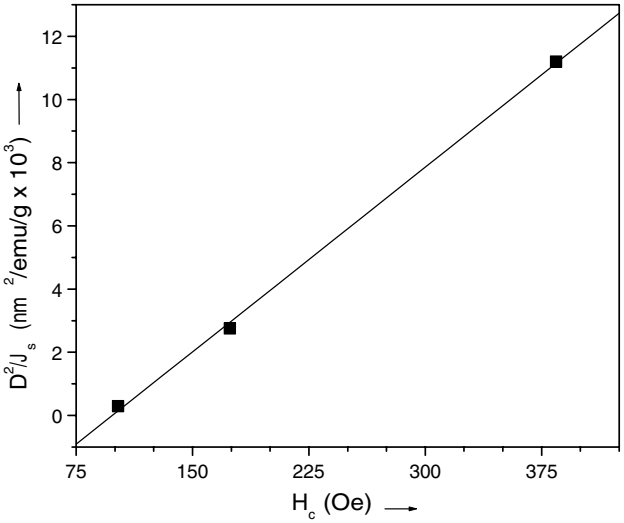

Figure 9. Verification of modified Herzer Law. Plot depicting variation of D^2/M_s versus H_c.

vapour pressures of the alloying elements one can infer that the deposited film has a lower volume fraction of molybdenum [18]. This can well account for the observed decrease in the crystallization temperatures. A detailed investigation of the phase compositions is in progress. However, at higher annealing temperatures small crystallite particles are precipitated increasing the number of domain walls. The inclination of the magnetization curve suggests that the major contribution of magnetization reversal is due to domain rotation. The relatively large coercivity of the thin films compared with bulk ribbons is due to the presence of localized stresses in the thin films which act as pinning centres for domain walls. Annealing ribbons at 373 K results in the nucleation of FeNi which is evident from the decrease in H_c after annealing at 373 K. The coercivity reaches a minimum at 473 K suggesting the onset of nano-crystallization and thereafter increases monotonically by orders of magnitude and reaches a maximum at around 673 K indicating grain growth with temperature. The coercivity minimum at 673 K suggests that the films undergo substantial stress relief and occurrences of nano-crystallization at that temperature. The slope of H_c after 473 K ensures that the size and volume fraction of the precipitates increase at a proportional rate. At 473 K FeNi nano-grains become exchange coupled and magneto-crystalline anisotropies are averaged out resulting in very low coercivity. The increase in grain size and modifications in the local stress within the material account for the increase in coercivity as the crystalline volume fraction increases at higher annealing temperatures. The second crystallization stage increases the volume fraction of boride phases whose presence is deleterious for the soft magnetic properties. This accounts for the decrease in M_s and increase in H_c values at higher annealing temperatures.

These variations can be explained by invoking the random anisotropy model originally suggested by Alben *et al* and modified by Herzer [19]. According to this model the ferromagnetic exchange length L_{ex} characterizes the exchange coupling between the grains:

$$L_{ex} = \sqrt{\frac{A}{K_1}}. \tag{2}$$

Here A represents the exchange stiffness constant, which is a characteristic parameter in magnetism, K_1 the uniaxial anisotropy and L_{ex} the exchange correlation length . When the exchange correlation length overwhelms the structural correlation length the anisotropies are averaged over several domains. If N such domains are in the volume L_{ex}^3, then it follows that

$$\langle K \rangle = \frac{K_1}{\sqrt{N}} = K_1 \left(\frac{D}{L_{ex}} \right)^{3/2}, \tag{3}$$

where $\langle K \rangle$ is the mean fluctuation amplitude of the anisotropies and D the average grain size.

Combination of equations (2) and (3) gives

$$\langle K \rangle = \frac{K_1^4}{A^3} D^6, \tag{4}$$

which suggests that the mean anisotropy is scaled by the sixth cube root of the average grain size. The coercivity is found to be related to the sixth power of grain size as

$$H_c = \frac{p_c \langle K \rangle}{M_s} = p_c \frac{K_1^4 D^6}{M_s A^3}. \tag{5}$$

In the above equation p_c serves as a fitting parameter and M_s is the saturation magnetization. These equations serve well for the three-dimensional cases. Typical values of (L_{ex}) for a metallic glass with $K_1 \approx 6\,\mathrm{kJ\,m^{-3}}$ and $A \approx 10^{-11}\,\mathrm{J\,m^{-3}}$ turns out to be $\approx$ 40 nm. In bulk metallic glasses if the nanocrystalline grain size is less than the exchange correlation lengths ($\approx$ 40 nm) the anisotropies are averaged out over several grains and the sample exhibits good soft magnetic properties. But when one of the dimensions is restricted to very low values (<40 nm) the system can very well be approximated to a two-dimensional system. In such a case the averaging effect is confined to two dimensions and the above equations

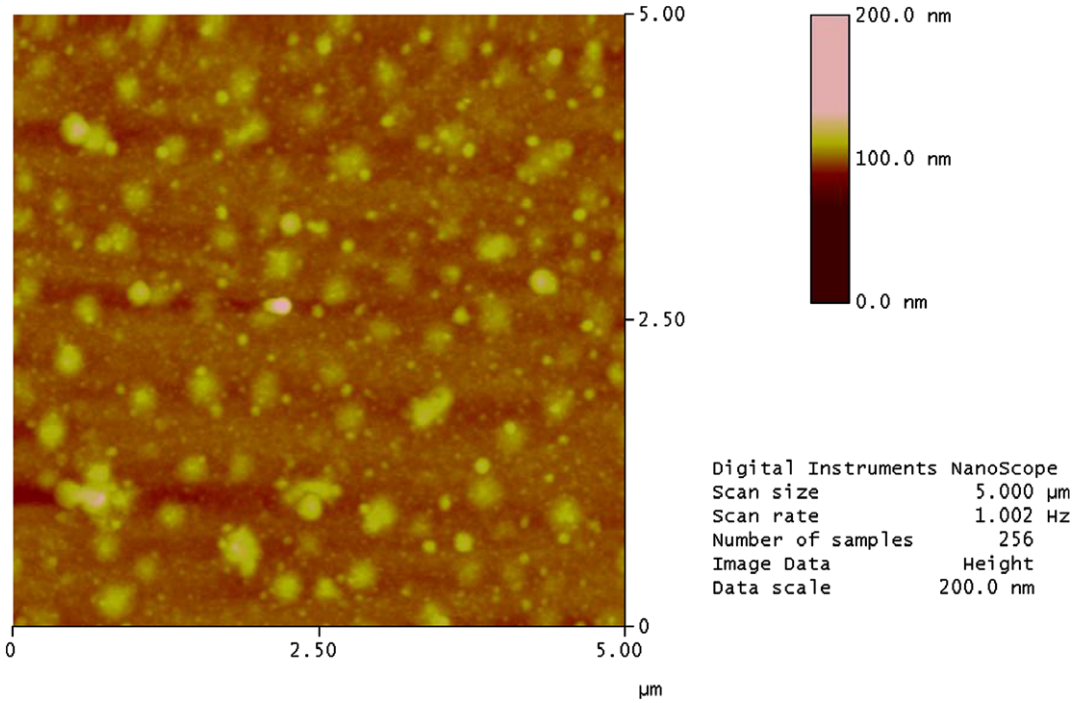

Figure 10. AFM image of pristine thin film.

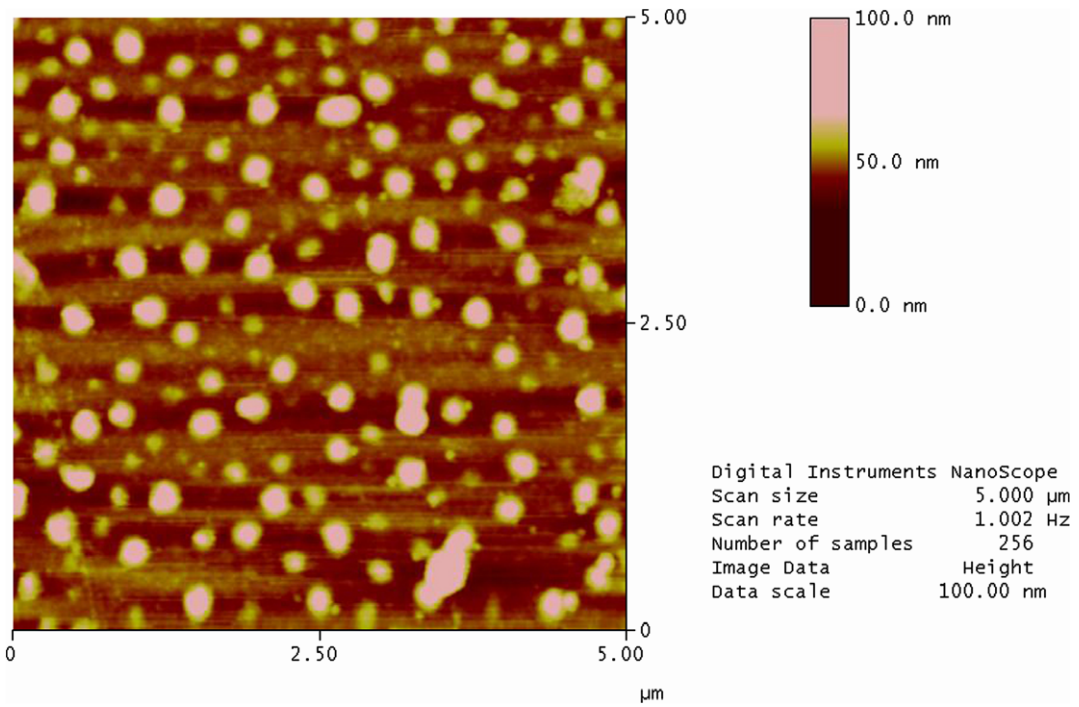

Figure 11. AFM Image of thin film annealed at 573 K.

can be modified as

$$\langle K \rangle = \frac{K_1^2}{A} D^2, \tag{6}$$

$$H_c = \frac{p_c \langle K \rangle}{M_s} = p_c \frac{K_1^2 D^2}{M_s A}, \tag{7}$$

where all the parameters in the equations have their usual meaning except the fact that they are the two-dimensional counterparts of the three-dimensional values. This equation suggests that for ultra-thin films the Herzer's D^6 law has to be replaced with D^2 law. The coercivity H_c is directly proportional to (D^2/M_s). The linear plot of D^2/M_s versus H_c is shown in figure 9 and confirms that the coercivity indeed obeys D^2 behaviour rather than D^6 behaviour.

The micro-structural analysis carried out on pristine and annealed samples is in good conformity with the results

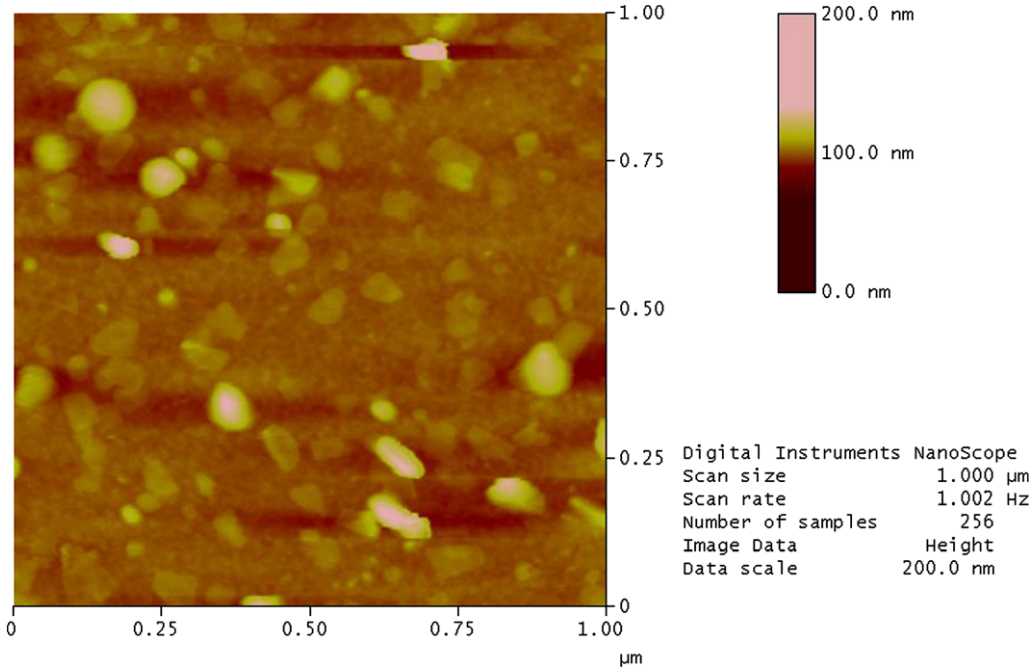

Figure 12. AFM image of thin film annealed 673 K.

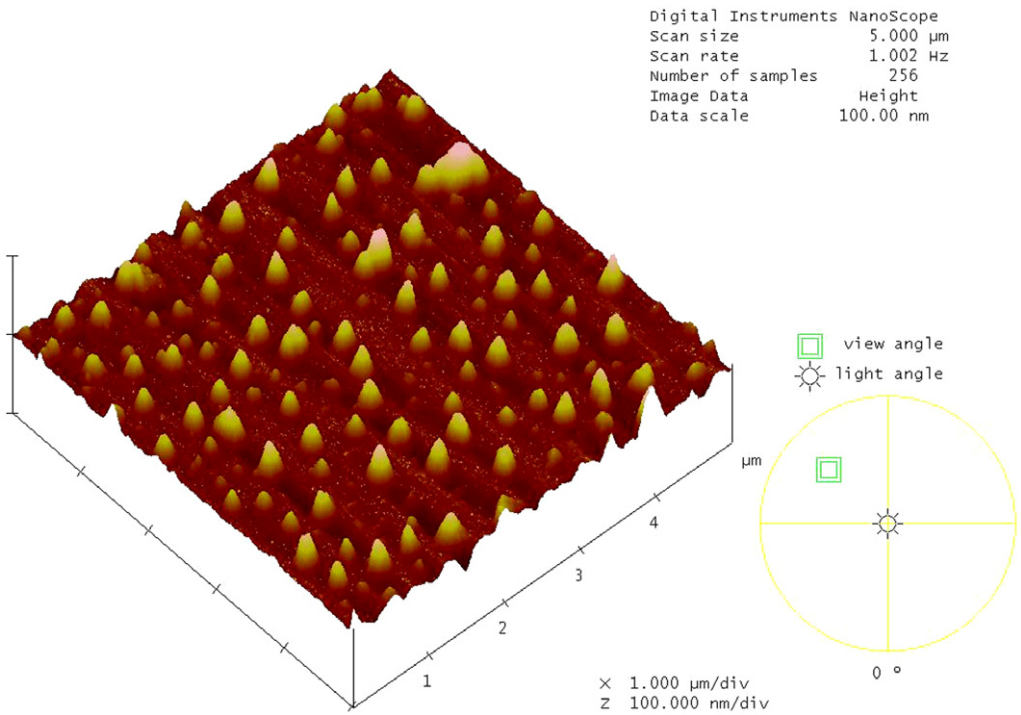

Figure 13. Three-dimensional MFM image of the thin film annealed at 573 K.

obtained from VSM studies. From XRD and AFM images (figures 10–12) it is clear that the as-deposited films are amorphous. Clusters are found in the AFM image of pristine and annealed samples which are magnetic, as evidenced from MFM (figure 13). Obviously these are Fe–Ni clusters. This clustering arises due to variation in vapour pressures of the alloying components. Fe and Ni having low vapour pressures evaporate slowly in the beginning and later on when the melt is deficient in boron, the rate increases. This accounts for the clustering of Fe–Ni on the film surface. The 473 K annealed samples show crystallites, which show good magnetic response with well-defined grains arranged uniformly over the film. But annealing at higher temperatures results in the crystallization of the amorphous matrix. The AFM of 673 K annealed samples show crystallites with varied morphology and shape. Hence, it is evident that the vapour deposition of metglas has resulted in the decrease of the crystallization temperatures of two phases. Crystallization of the first phase occurs at 473 K

and the second crystallization occurs at 673 K. From MFM it was found that the samples are magnetic up to an annealing temperature of 573 K and thereafter the magnetic properties deteriorate.

4. Conclusions

It has been found that the temperature of annealing can modulate the magnetic properties of metglas alloys and thin films. Thin film Samples annealed at 473 K show very low coercivity and large saturation magnetization suggesting that the critical condition predicted by the Herzer model is attained at this temperature. The XRD spectrum of thin films annealed at 473 K shows that Fe–Ni nanostructures are embedded in the residual boron rich amorphous phase. Annealing ribbons at higher temperatures resulted in a monotonic increase in coercivity and magnetization because of micro-structural changes. Finally, an explanation is provided for coercivity variation with annealing based on the modified Herzer model. There exists ample scope for the modelling and simulation of the magnetic evolution of ultra-thin films using this new model. Thin films of these metglas ribbons can find many applications involving soft magnetic properties.

Acknowledgment

MRA and HT acknowledges Nuclear Science Centre, New Delhi, for providing financial assistance in the form of a project (No UFUP-35306).

References

[1] Hesegava R and ÕHandley R C 1979 *J. Appl. Phys.* **50** 1551
Herzer G 1997 *Proc. NATO Advanced Study institute on Magnetic Hysteresis in Novel Materials (Greece)* ed George C Hadjipanayis (London: Kluwer) p 711
Du S W and Ramanujan R V 2005 *J. Non-Cryst. Solids* **351** 3105
[2] Saiseng S, Wintai P, Nilpairuch S, Limsuwan P and Tang I M 2004 *J. Magn. Magn. Mater.* **278** 172
[3] Shirae S 1979 *J. Appl. Phys.* **50** 7618
[4] Du S W and Ramanujan R V 2004 *Metastable Nanocryst. Mater.* **23** 207
[5] Hesagava R, Narasimhan M C and DeCristofara N 1978 *J. Appl. Phys.* **49** 1712
[6] Li J, Su Z, Wang T M, Hage S, Hahn H and Shirai Y 1999 *J. Mater. Sci.* **34** 111
[7] Das V D and Lakshmi J 1988 *Phys. Rev.* B **37** 720
[8] Greneche J M 2003 *J. Optoelectron. Adv. Mater.* **5** 133
[9] Chaudhury Z A and Suryanarayana C 1982 *Thin Solid Films* **98** 233
[10] Alben R, Becker J J and Chi M C 1978 *J. Appl. Phys.* **49** 1653
[11] Herzer G 1989 *IEEE. Trans. Magn.* **25** 3327
[12] Hristoforou E 2002 *J. Optoelectron. Adv. Mater.* **4** 245
[13] Kissinger H E 1957 *Anal. Chem.* **29** 57 1702
[14] Raja V S, Kishore and Ranganathan S 1987 *Bull. Mater. Sci.* **9** 207
[15] Du S W and Ramanujan R V 2004 *Mater. Sci. Eng.* A **75** 1040
[16] Nicolai H P, Kopmann G and Frommeyer G 1981 *Z. Metallk.* **72** 558
[17] Jyothi M and Suryanarayana C 1985 *Z. Metallk.* **76** 802
[18] Seshu B, Bhatnagar A K and Naugle D G 1997 *J. Mater. Sci. Lett.* **16** 165
[19] Herzer G 1990 *IEEE Trans. Magn.* **26** 1397
Herzer G 1991 *Mater. Sci. Eng.* A **133** 1